ORIGINAL PAPER

Nonlinear vibration suppression of composite laminated beam embedded with NiTiNOL-steel wire ropes

Li-Heng Zheng · Ye-Wei Zhang · Hu Ding · Li-Qun Chen

Abstract NiTiNOL-steel wire rope (NiTi-ST) is a new vibration absorber with nonlinear stiffness and hysteretic damping. Although there are many studies on NiTi-ST nonlinear identification, there are few studies on vibration suppression for laminated structures with NiTi-ST. In the present work, the NiTi-ST is integrated with a composite laminated beam for structural vibration suppression for the first time. A coupling model of the composite laminated beam embedded with NiTi-ST is proposed. The nonlinear restoring force and hysteretic damping force of NiTi-ST are processed into polynomial form. The responses of the beam embedded with different NiTi-ST are investigated by the Galerkin discretization together with the harmonic balance method (HBM). The terms of the polynomial model are discussed. Two numerical methods are utilized for steady-state responses and numerical validations. Simulation results demonstrate the effectiveness of NiTi-ST. This vibration suppression method can be popularized for other laminated structures and contribute to vibration control in engineering fields.

1 Introduction

Composite laminated beams are common structures for load-bearing and strength enhancement in industries. In the critical environment, a primary concern of the structure is the vibration caused by external loads or self-motions, which may lead to the reduction of the system's lifespan. Hence, the vibration suppression problem of composite laminated structures is significant.

Passive vibration absorption methods are widely used in engineering. In recent years, there has been great interest in nonlinear vibration suppression for composite beams and other structures. The common vibration control techniques are applying nonlinear passive control devices because they are simply designed, economical, and practical. The nonlinearity of these devices can increase the bandwidth of vibration suppression [1] and enhance the robustness of the system. To date, many studies have investigated the new design of passive nonlinear vibration absorbers and their applications. For example,

L.-H. Zheng · Y.-W. Zhang (✉) · H. Ding · L.-Q. Chen
Shanghai Institute of Applied Mathematics and Mechanics, Shanghai Key Laboratory of Mechanics in Energy Engineering, School of Mechanics and Engineering Science, Shanghai University, Shanghai 200072, China
e-mail: zhangyewei1218@126.com

Y.-W. Zhang
Faculty of Aerospace Engineering, Shenyang Aerospace University, Shenyang 110136, China

nonlinear vibration absorbers and isolators based on saturation phenomenon [2, 3], magnetism [4], and inerter [5] were proposed and thoroughly investigated. Various kinds of impact dampers were designed and analyzed for resonance suppression [6, 7]. One of the most representative nonlinear vibration absorbers is the nonlinear energy sink which can realize the targeted energy transfer [8–10] and achieve vibration suppression at various temperatures and moisture levels [11]. The nonlinear energy sink was applied to many structures such as linear systems [12, 13], beams [14, 15], laminated plates [16–18], and trapezoidal wings [19]. Overall, these studies highlight the massive need for better vibration suppression devices and strategies for engineering structures. The requirement of new passive vibration absorbers still exists.

Shape memory alloys (SMA) have many extraordinary properties such as complete shape recovery after experiencing large strains and energy dissipation through hysteresis of response [20]. Paiva et al. discussed the constitutive modeling of SMAs including polynomial models, models with assumed phase transformation kinetics, and models with internal constraints [21]. Savi et al. investigated the nonlinear dynamics of SMA systems and observed periodic, quasi-periodic, and chaotic behaviors [22, 23]. SMAs attracted the interest of many researchers in vibration control and structural engineering over the past decades. Ghasemi et al. used the SMA pounding tuned mass damper to control the wave-induced vibrations of the offshore jacket platforms [24]. Kumbhar et al. proposed an adaptive tuned vibration absorber based on magnetorheological elastomer-shape memory alloy composite and studied the dynamic response of the system with this absorber [25]. Huang et al. applied an SMA-based tuned mass damper to a timber floor system for semi-active control [26]. Qian et al. experimentally investigate structural vibration suppression under strong seismic excitation with a new super-elastic shape memory alloy friction damper [27]. The integration of SMAs into composite structures has resulted in many benefits, which include actuation, vibration control, damping, sensing, and self-healing [28]. Alebrahim et al. studied the thermomechanical properties of a hybrid composite beam with carbon fibers and SMA wires numerically and experimentally [29]. Bayat and EkhteraeiToussi analyzed the vibrations of a composite beam with SMA wires using the Panico–Brinson

model and differential quadrature-integral quadrature combined method [30, 31]. Soltanieh et al. investigated SMA wires embedded in composite plates with nonlinear finite element method and reported that SMA wires cannot always strengthen the plates [32]. Previous studies demonstrated that SMAs are great materials for new vibration absorbers. Short ropes can also dissipate energy when forced to deform bending due to the interwire friction. They have been widely used for vibration isolation [33] and tuned mass damper [34]. A new nonlinear vibration absorber made of assemblies of nickel titanium-Naval Ordnance Laboratory (NiTiNOL) strands, wires, and steel wire ropes was proposed by Carboni et al. [35]. The NiTiNOL-steel wire ropes (NiTi-ST) with multiple configurations were theoretically and experimentally analyzed, and the hysteresis was described with a modified Bouc–Wen model [36]. There are mainly two methods for modeling hysteresis: one is based on physical hysteresis characters, and the other is based on hysteresis phenomenology [37]. The phenomenological models are merely mathematical models, and they can describe different hysteresis loops more generally. There are operator-based models and differential-based models [38]. Bouc–Wen model is one of the most popular differential-based models with a strong ability in describing hysteresis loops with different trigonometric features [39]. Bouc–Wen model has widespread applications in structural elements, mechanical systems, energy dissipation systems, and so on. The modified Bouc–Wen model proposed by Carboni et al. [36] took account of the pinching behavior of NiTi-ST. The nonlinear dynamic behavior character of NiTi-ST was investigated in the frequency domain and time domain, and the absorber properties were optimized [40]. The NiTi-ST can be used for multiple purposes. Carboni et al. evaluated the NiTi-ST in a structure of multistory steel building model which demonstrated a good performance within designed frequency bandwidth [41]. Zhang et al. [42] developed a novel NES with NiTi-ST for whole-spacecraft vibration isolation.

Despite the rich dynamic behavior of the device, the NiTi-ST still requires robust mechanic models for analysis. The nonlinear parametric identification of NiTi-ST poses a considerable challenge to the research community. Carboni et al. [43] identified the parameters of the modified hysteretic restoring force model to minimize the difference between

numerical and experimental results. Brewick et al. [44] employed data-driven methodologies to create a generalized model for NiTi-ST. The experiment data were identified with Volterra/Wiener neural network, polynomial basis methods, and artificial neural networks. The results indicated that the polynomial model can represent the nonlinear behaviors of NiTi-ST. Combined with naïve elastic net regularization, Brewick et al. reduced the order of the polynomial model and obtained comparable results of traditional methods [45]. Currently, most researchers are dedicated to parametric identification of NiTi-ST. The applications on composite structures are rarely presented, and the strong ability to suppress vibration of composite beams is rarely reported, to the authors' best knowledge.

With the reduced-order polynomial model for NiTi-ST proved to be suitable for reporting the dynamic behavior briefly, in the present paper, the NiTi-ST coupled to a composite laminated beam is studied via semi-analytical and numerical methods for the first time. The nonlinear restoring and damping forces of NiTi-ST are converted into reduced-order polynomial models. It is noted that the real SMA devices exhibit strong thermomechanical coupling [46]. The difference between nonisothermal and isothermal behavior can be pronounced when the mechanical load is changing rapidly [47]. In the present paper, to simplify modeling, the composite beam embedded with NiTi-ST is investigated under the isothermal condition and the thermomechanical behavior is ignored. The nonlinear responses of the beam are obtained, and the vibration suppression effects of the NiTi-ST are examined. The rest of the paper is arranged as follows: In Sect. 2, a 1-DOF system with NiTi-ST is presented for polynomial model fitting. The composite beam model is established, and the polynomial model is coupled as the nonlinear restoring and damping force. In Sect. 3, the Galerkin truncation method is used to discretize the nonlinear governing equation of the beam and the HBM [48] combined with the presto-arc length method [49] is used to obtain the semi-analytical results. In Sect. 4, a modified variational approach [50, 51] is developed to establish the discretized beam model. The Newmark-β method is employed for nonlinear time-domain responses. The Runge–Kutta method is carried out to verify the results in Sects. 3 and 4. It is found that the NiTi-ST is a promising vibration absorber for the composite beam.

The NiTi-ST may have a bright future in engineering applications.

2 Modeling of the system

The coupled system is made of a slender laminated beam with length L, width B, and height h and NiTi-ST damper. The NiTi-ST is glued onto the composite beam with composite adhesive and fully fixed to the upper surface of the beam, as shown in Fig. 1. The beam is simply supported at the end of both sides.

2.1 Restoring and damping force model of NiTi-ST with validation

Considering the transverse vibration of the beam, the restoring and damping force f_{st} provided by NiTi-ST [36] can be expressed as

$$f_{st} = (1 - r)k_c w^3 + r(k_e w + z_h) \tag{1}$$

where w is the generalized displacement field at the middle surface of the beam. The nonlinear restoring and damping force f_{st} is related to the displacement field of the beam. r, k_c, k_e are parameters obtained by experiments. z_h is a hysteresis damping force described as a modified Bouc–Wen model:

$$\begin{cases} \dot{z}_h = \{k_d h(x) - (\gamma + \beta \text{sgn}(z_h \dot{w}))|z_h|^n\}\dot{w} \\ h(x) = 1 - \xi e^{-\frac{w^2}{w_c}} \end{cases} \tag{2}$$

where k_d, γ, β, n, ξ, w_c are material parameters, $\dot{z}_h$ is the first-order differentiation of z_h concerning time, $h(x)$ is the pinching function for modulating the tangent stiffness at the origin. Table 1 lists the parameter values of different NiTi-ST configurations.

The restoring and damping force f_{st} is distributed at the middle surface of the beam with the form of differential equations, which are hard to be dealt with. Hence, based on the thought of restoring force surface
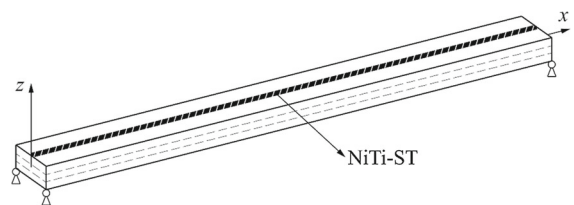

Fig. 1 Composite beam embedded with NiTi-ST

Table 1 Parameter values of different NiTi-ST configurations Snj [40]

Snj	$k_c \left(\frac{kN}{mm^3}\right)$	$k_e \left(\frac{kN}{mm}\right)$	$k_d \left(\frac{kN}{mm}\right)$	$\gamma \left(\frac{kN^{-n+1}}{mm}\right)$	$\beta \left(\frac{kN^{-n+1}}{mm}\right)$	n (–)	ξ(–)	w_c(mm^2)	r (–)
S1a	4.611×10^{-4}	0.010	1.00	0.400	0.349	1.0	0.99	277.72	0.251
S2a	–	5.250×10^{-3}	0.020	0.500	0.544	1.0	–	–	1
S2b	–	4.17×10^{-3}	0.0684	0.500	1.5	1.0	0.674	950	1
S3a	4.647×10^{-5}	0.017	0.163	0.878	1.441	1.1	0.896	78.81	0.308
S3b	9.978×10^{-5}	0.013	0.460	1.204	1.219	1.1	0.755	234.33	0.321
S3c	1.638×10^{-4}	0.010	0.034	0.334	1.288	1.118	0.208	57.37	0.739

method, the force f_{st} is identified into a polynomial function. To start polynomial fitting, the force–displacement–velocity data of NiTi-ST are essential, which can be obtained from the modified Bouc–Wen models. Therefore, a lumped-mass 1-DOF system shown in Fig. 2 is proposed to provide polynomial fitting data. Assuming that the force f_{st} is proportional to the force provided by NiTi-ST of a 1-DOF system. The force f_{st} is proportional to the force provided by NiTi-ST of a 1-DOF system. The rigid mass m moves along the vertical direction. The excitation force is expressed as $F_0 \sin(2\pi f_0 t)$. Engorging the gravity effect of the mass m and the NiTi-ST, the governing equation is given as:

$$m\ddot{w}_m = F_0 \sin(2\pi f_0 t) - f_{st} \tag{3}$$

where w_m represents the displacement of the mass m. It should be noted that the displacement w_m is different with the displacement field of the composite beam. The displacement field of the beam is related to the position of the beam. Substituting Eqs. (1) (2) into Eq. (3), the dynamic equation can be solved with Runge–Kutta method. After obtaining the time-domain response of the 1-DOF system, the data of the last five periods are chosen for fitting.

↑ Excitation force

m
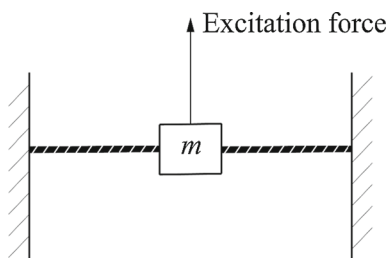
Fig. 2 A 1-DOF system restricted with NiTi-ST

The data obtained above are imported into the curve fitting toolbox of MATLAB. A polynomial function is proposed to capture the nonlinearity of the restoring and damping force. The polynomial function is of the displacement w and the velocity $\dot{w}$ of the system. While polynomial-based models are moderately accurate, they are simple to implement and allowed for reduced-order modeling [44]. Since the analytical results of the responses are required next, polynomial models are necessary.

In an attempt to simplify the expression of the restoring and damping force model as much as possible, the maximum order of nonlinear terms is set to be 3. After removing several terms with little influence on the fitting results, a polynomial function basis with no more than five terms is used for fitting, which can be expressed as

$$f_{st} = k_1 w + k_3 w^3 + c_1 \dot{w} + r_{21} w^2 \dot{w} + r_{12} w \dot{w}^2 \tag{4}$$

where k_1, k_3, c_1, r_{21}, and r_{12} are stiffness coefficient and nonlinear damping coefficients. The curve fitting results are listed in Table 2.

Next, validation of the identified model is carried out. The force of the Bouc–Wen model in the 1-DOF system is replaced with the restoring and damping force of the polynomial fitting model. The restoring and damping force behavior is obtained, as presented in Fig. 3. The identified model reports acceptable results for all configurations. For configuration S1a, the polynomial model managed to capture the nonlinear cubic stiffness. The restoring and damping forces of configuration S2a and S2b are not accurately identified. The sharp corners of the hysteresis loops cannot be described with reduced-order polynomial models because the hysteresis damping is replaced with polynomial damping terms in the identified model.

Table 2 Parameter values of identified restoring and damping force model

Snj	$k_1 \left(\dfrac{\text{N}}{\text{m}}\right)$	$\bar{k}_3 \left(\dfrac{\text{N}}{\text{m}^3}\right)$	$c_1 \left(\dfrac{\text{N s}}{\text{m}}\right)$	$r_{21} \left(\dfrac{\text{N s}}{\text{m}^3}\right)$	$r_{12} \left(\dfrac{\text{N s}^2}{\text{m}^3}\right)$	R-Square
S1a	–	4.097×10^8	122.4	1.699×10^6	-6.515×10^4	0.9983
S2a	5966	–	52.09	1.259×10^5	-9876	0.9986
S2b	4523	–	16.49	1.077×10^5	-2608	0.9963
S3a	6016	3.228×10^7	49.96	3.396×10^5	-2.26×10^4	0.9996
S3b	3962	7.299×10^7	124.70	6.446×10^5	-2.998×10^4	0.9989
S3c	8535	4.222×10^7	104.80	6.114×10^4	-2.761×10^4	0.9999

Fig. 3 Force–displacement loops for different NiTi-ST configurations: **a** S1a, **b** S2a, **c** S2b, **d** S3a, **e** S3b and **f** S3c
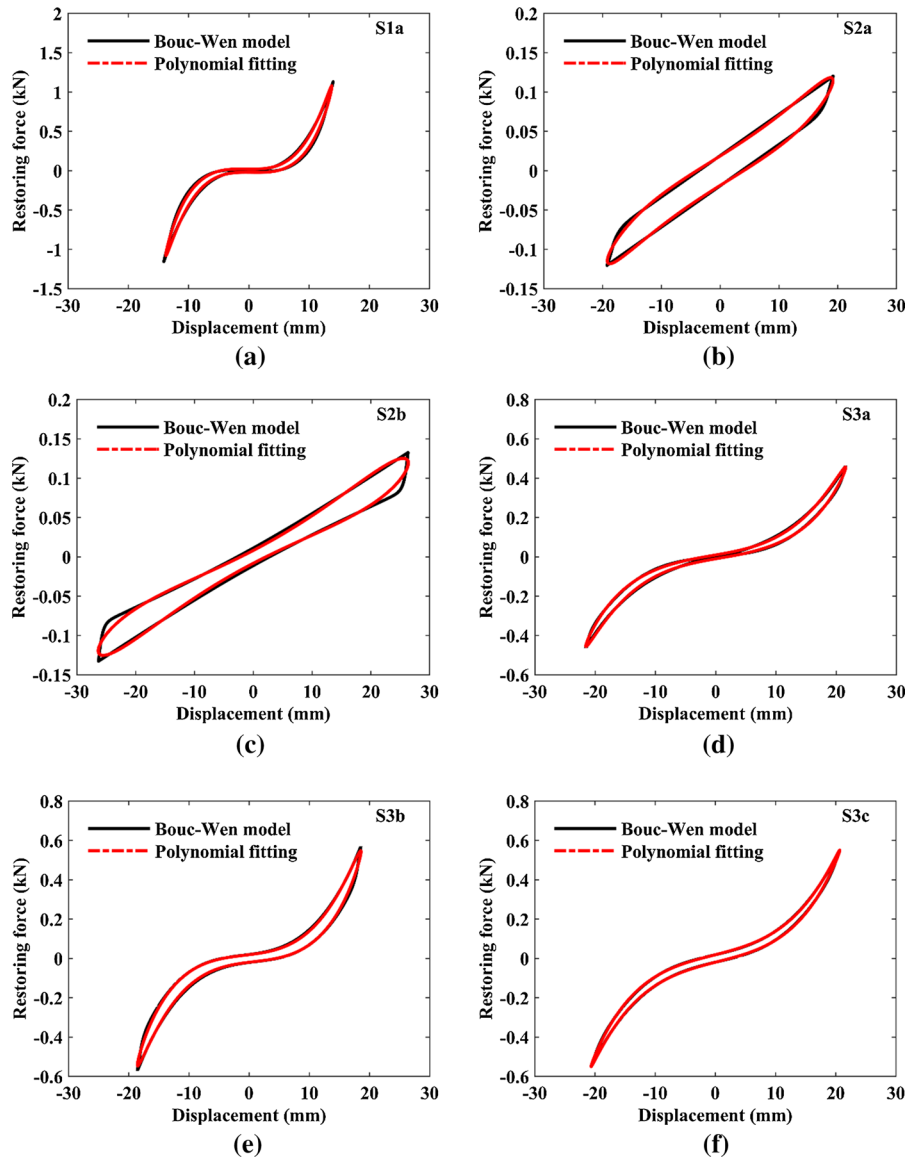
Higher order damping terms are required for more accurate descriptions. For the rest of the configurations, the identified polynomial model performs relatively better than S2a and S2b. The identified restoring and damping force model is applied for the rest of the modeling.

2.2 Composite beam model

The composite laminated beam with N_l layers is studied. The coordinates of kth lamina on the z-axis are z_k and z_{k+1}. Based on the Euler–Bernoulli beam model, displacement functions of an arbitrary point in the beam can be written as

$$\begin{cases} \tilde{u}(x,z,t) = -z \dfrac{\partial w}{\partial x} \\ \tilde{w}(x,z,t) = w(x,t) \end{cases} \tag{5}$$

where $\tilde{u}$ and $\tilde{w}$ are the displacement of the arbitrary point in x- and z-directions, respectively. w is the generalized displacement at the middle surface of the beam. The generalized displacement field w differs from the displacement w_m of the lumped-mass system in Fig. 2. It is related to the position x of the beam.

The normal strain of the composite laminated beam can be expressed as

$$\varepsilon_{xx} = -z \frac{\partial^2 w}{\partial x^2} \tag{6}$$

The constitutive equation of the kth layer can be expressed as follows

$$\begin{bmatrix} \sigma_{xx} \\ \sigma_{yy} \\ \sigma_{xy} \end{bmatrix}^{(k)} = \begin{bmatrix} \overline{Q}_{11}^{(k)} & \overline{Q}_{12}^{(k)} & \overline{Q}_{16}^{(k)} \\ \overline{Q}_{12}^{(k)} & \overline{Q}_{22}^{(k)} & \overline{Q}_{26}^{(k)} \\ \overline{Q}_{16}^{(k)} & \overline{Q}_{26}^{(k)} & \overline{Q}_{66}^{(k)} \end{bmatrix} \begin{bmatrix} \varepsilon_{xx} \\ \varepsilon_{yy} \\ \gamma_{xy} \end{bmatrix}^{(k)} \tag{7}$$

where $\overline{Q}_{i,j}^{(k)}(i,j=1,2,6)$ denotes the transformed elastic coefficient related to the kth lamina elastic constants $Q_{i,j}^{(k)}$ and the angle $\theta^{(k)}$ between the x-axis and the principal material directions. It can be calculated with the following expression:

$$\overline{Q}_{11}^{(k)} = Q_{11}^{(k)} \cos^4 \theta^{(k)} + 2\left(Q_{12}^{(k)} + 2Q_{66}^{(k)} \right)$$
$$\sin^2 \theta^{(k)} \cos^2 \theta^{(k)} + Q_{22}^{(k)} \sin^4 \theta^{(k)}$$
$$\overline{Q}_{12}^{(k)} = \left(Q_{11}^{(k)} + Q_{22}^{(k)} - 4Q_{66}^{(k)} \right) \sin^2 \theta^{(k)} \cos^2 \theta^{(k)}$$
$$+ Q_{12}^{(k)} \left(\sin^4 \theta^{(k)} + \cos^4 \theta^{(k)} \right)$$
$$\overline{Q}_{22}^{(k)} = Q_{11}^{(k)} \sin^4 \theta^{(k)} + 2\left(Q_{12}^{(k)} + 2Q_{66}^{(k)} \right)$$
$$\sin^2 \theta^{(k)} \cos^2 \theta^{(k)} + Q_{22}^{(k)} \cos^4 \theta^{(k)}$$
$$\overline{Q}_{16}^{(k)} = \left(Q_{11}^{(k)} - Q_{12}^{(k)} - 2Q_{66}^{(k)} \right) \sin \theta^{(k)} \cos^3 \theta^{(k)}$$
$$+ \left(Q_{12}^{(k)} - Q_{22}^{(k)} + 2Q_{66}^{(k)} \right) \sin^3 \theta^{(k)} \cos \theta^{(k)}$$
$$\overline{Q}_{26}^{(k)} = \left(Q_{11}^{(k)} - Q_{12}^{(k)} - 2Q_{66}^{(k)} \right) \sin^3 \theta^{(k)} \cos \theta^{(k)}$$
$$+ \left(Q_{12}^{(k)} - Q_{22}^{(k)} + 2Q_{66}^{(k)} \right) \sin \theta^{(k)} \cos^3 \theta^{(k)}$$
$$\overline{Q}_{66}^{(k)} = \left(Q_{11}^{(k)} + Q_{22}^{(k)} - 2Q_{12}^{(k)} - 2Q_{66}^{(k)} \right) \sin^2 \theta^{(k)}$$
$$+ Q_{66}^{(k)} \left(\sin^4 \theta^{(k)} + \cos^4 \theta^{(k)} \right)$$
$$\tag{8}$$

The elastic constants $Q_{i,j}^{(k)}$ can be expressed from the engineering elastic parameters of the kth material:

$$Q_{11}^{(k)} = \frac{E_1^{(k)}}{1 - \mu_{12}^{(k)} \mu_{21}^{(k)}}, \quad Q_{12}^{(k)} = \frac{\mu_{12}^{(k)} E_2^{(k)}}{1 - \mu_{12}^{(k)} \mu_{21}^{(k)}},$$
$$Q_{22}^{(k)} = \frac{E_2^{(k)}}{1 - \mu_{12}^{(k)} \mu_{21}^{(k)}}, \quad Q_{66}^{(k)} = G_{12}^{(k)} \tag{9}$$

The external load is uniformly distributed over an area with $x_1 = L/4$ and $x_2 = L/2$ on the upper surface of the beam, seeing Fig. 4.

According to the generalized Hamilton's principle, the governing equation of the composite beam can be obtained by
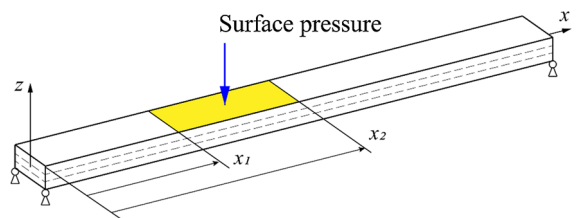

Fig. 4 Excitation applied on the beam

$$\delta \int_{t_1}^{t_2} \left(T - U + W_f + W_{st} \right) \mathrm{d}t = 0 \tag{10}$$

where T, U, W_f, and W_{st} are the potential energy, the kinetic energy, the work done by the restoring and damping force provided by NiTi-ST, and the work done by external loads, respectively, given as:

$$\begin{cases} T = \dfrac{1}{2} \sum_{k=1}^{N_l} \int_{z_k}^{z_{k+1}} \int_S \rho^{(k)} \dot{w}^2 B \, \mathrm{d}x \, \mathrm{d}z \\ U = \dfrac{1}{2} \int_0^L N_x \dfrac{\partial^2 w}{\partial x^2} B \, \mathrm{d}x \\ W_f = \int_0^L B f_w(x) w \, \mathrm{d}x \\ W_{st} = \int_0^L -\chi f_{st} w \, \mathrm{d}x \end{cases} \tag{11}$$

with $\rho^{(k)}$, N_x, f_w, χ representing the density of kth lamina, the generalized force resultant of the beam, the external loads distributed on the x-axis, and the parameter modifying the restoring and damping force. N_x can be written as:

$$N_x = \sum_{k=1}^{N_l} \int_{z_k}^{z_{k+1}} -z \sigma_{xx} \mathrm{d}z \tag{12}$$

Substituting Eqs. (4) and (11) into Eq. (10) and setting the coefficients of virtual displacements to zero yield

$$\begin{aligned} &\rho B h \ddot{w} + B \frac{\partial^2 N_x}{\partial x^2} + \eta B \frac{\partial^3 N_x}{\partial x^2 \partial t} \\ &= B f_w \\ &\quad - \chi \left(k_1 w + k_3 w^3 + c_1 \dot{w} + r_{21} w^2 \dot{w} + r_{12} w \dot{w}^2 \right) \end{aligned} \tag{13}$$

Equation (13) is reduced by assuming that the thickness, density, and strain of every lamina are the same, respectively. The layers of the laminated beam are cross-ply (0°/90°/0°/90°). The geometry dimensions of the beam are length L = 0.462 m, width $B = L/15$, height $h = L/50$, and the material properties are E_1 = 152.4 GPa, E_2 = 10.16 GPa, $G_{12} = G_{13}$ = 4.36 GPa, G_{23} = 3.75 GPa, γ_{12} = 0.3 and ρ = 1461.73 kg/m^3. The damping coefficient $\eta = 10^{-5}$, and the parameter modifying the restoring and damping force $\chi = 0.2$.

3 Analytical solutions

3.1 Galerkin truncation

The Galerkin method is one of the most common procedures for truncating the partial differential equation. Based on the simply supported boundary conditions, the solution of Eq. (13) is written as:

$$w(x, t) = \sum_{i=1}^n q_i(t) \cdot \sin \frac{i \pi x}{L} \tag{14}$$

where i is the order of the modal shape function. Once substituting Eq. (14) into Eq. (13), according to the Galerkin method with four modes, the equation can be transformed into Eq. (15):

$$\begin{aligned} &\int_0^L \sum_{i=1}^n \left(\rho B h \ddot{w} + B \frac{\partial^2 N_x}{\partial x^2} + \eta B \frac{\partial^3 N_x}{\partial x^2 \partial t} \right) \cdot \sin \frac{i \pi x}{L} \mathrm{d}x \\ &- \int_0^L \sum_{i=1}^n \left(B f_w - \chi \left(k_1 w + k_3 w^3 + c_1 \dot{w} + r_{21} w^2 \dot{w} + r_{12} w \dot{w}^2 \right) \right) \cdot \\ &\quad \cdot \sin \frac{i \pi x}{L} \mathrm{d}x = 0 \end{aligned} \tag{15}$$

Expanding Eq. (15) yields a set of ordinary differential equations:

$$\begin{aligned} &\eta_{1,i} \ddot{q}_i + \eta_{2,i} \dot{q}_i + \eta_{3,i} q_i - \eta_{4,i} f_w + \eta_{5,i} \\ &\quad \cdot \int_0^L \sum_{i=1}^n \chi \left(k_1 w + \overline{k}_3 w^3 + c_1 \dot{w} + r_{21} w^2 \dot{w} + r_{12} w \dot{w}^2 \right) \\ &\quad \cdot \sin \frac{i \pi x}{L} \mathrm{d}x = 0 \end{aligned} \tag{16}$$

where $\eta_{j,i}$ are the coefficients of the ODEs.

3.2 Harmonic balance method

The harmonic balance method combined with the presto-arc length method is adopted for the approximately analytical results. With the thought of harmonic balance, the displacement response can be expanded as

$$q_i(t) = A_{i,0} + \sum_{j=1}^{\hat{n}} \cos(j \omega t) \cdot C_{i,j} + \sum_{j=1}^{\hat{n}} \sin(j \omega t) \cdot S_{i,j} \tag{17}$$

with j as the harmonic order. The $A_{i,0}$, $C_{i,j}$, and $S_{i,j}$ are the constant terms, the coefficients of cosine and

sine terms, respectively. The velocity and acceleration responses are given as

$$\dot{q}_i(t) = -\sum_{j=1}^{\hat{n}} j\omega \sin(j\omega t) \cdot C_{i,j} + \sum_{j=1}^{\hat{n}} j\omega \cos(j\omega t) \cdot S_{i,j}$$

$$\ddot{q}_i(t) = -\sum_{j=1}^{\hat{n}} j^2\omega^2 \cos(j\omega t) \cdot C_{i,j} - \sum_{j=1}^{\hat{n}} j^2\omega^2 \sin(j\omega t) \cdot S_{i,j}$$

(18)

Since the order of the nonlinear restoring and damping force is 3, the constant terms and the second-order terms are omitted. The harmonic terms with $j = 1, 3$ remain and are substituted into Eq. (16). After balancing the coefficients of all the harmonic terms, a set of nonlinear algebraic equations related to the coefficients are obtained. Following the presto-arc length method, the amplitude–frequency response curve can be easily obtained.

3.3 Analytical results

The response is measured at the position of $3/4L$ on the x-axis. Figure 5 demonstrates the amplitude response of the composite beam. The natural frequency of the composite laminated beam is 146.3 Hz. As illustrated in Fig. 5a, the NiTi-ST successfully reduced the vibration amplitude around the natural frequency. The S3b configuration demonstrates the best result and the resonance frequency is hardly changed. The S1a and S3a configurations show slightly softening behavior. The softening behavior is caused by the quasi-zero stiffness of S1a and S3a around the origin. The restoring force provided by S1a configuration mainly consists of cubic stiffness restoring force, and the S3a is affected by the pinching effect. When the excitation

increases, as shown in Fig. 5b, S1a and S3a present jump phenomenon, while other configurations show softening behaviors which might be the contribution of hysteresis. Figure 6 presents the progress with the increment of the external load.

A parametric study is carried out for avoiding the jump phenomenon. In Fig. 7, the minus cubic term r_{12} is changed for S1a and S3b. As the absolute value of r_{12} decreased, the S1a configuration recovered. On the contrary, while increasing the absolute value of r_{12} for S3b, the jump phenomenon appears. It seems that the sudden increments of amplitude are caused by the flaws of reduced-order polynomial model rather than the nonlinearity of NiTi-ST. The polynomial models are only suitable for reporting nonlinear responses under reasonable excitation.

The equivalent linear damping c_I is also studied as shown in Fig. 8. With the increment of c_1, the ability of vibration reduction is enhanced, while the resonance frequency remains unchanged. The polynomial model contains many terms related to the velocity, while the equivalent damping term plays a major role in dissipating energy. Hysteresis damping features of NiTi-ST are described with other high-order terms, which contribute to energy dissipation less than linear damping c_1.

4 Numerical analysis

4.1 Domain decomposition

The domain decomposition approach is a truncation method based on the modified variational principle (MVP) and the least-square weight residual method

Fig. 5 Vibration suppression effect of different NiTi-ST configurations under small and large external loads: **a** f_w = 4 kPa, **b** f_w = 16 kPa. Legend 'Null' represents the response of composite beam without NiTi-ST
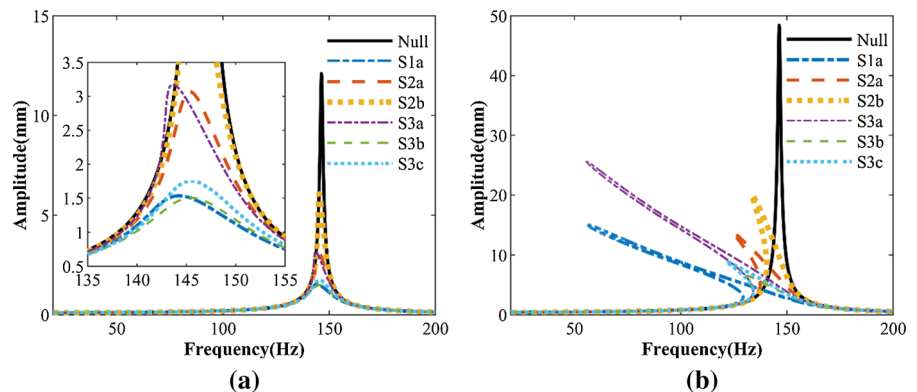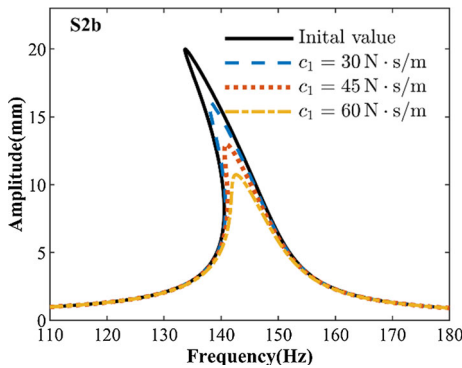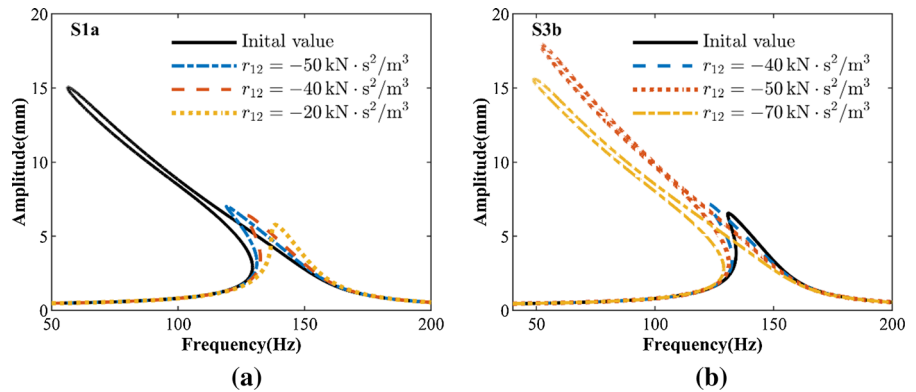
Fig. 6 Softening and unstable behavior of configurations with the increment of external load form 4 to 16 kPa: **a** S1a, **b** S3b
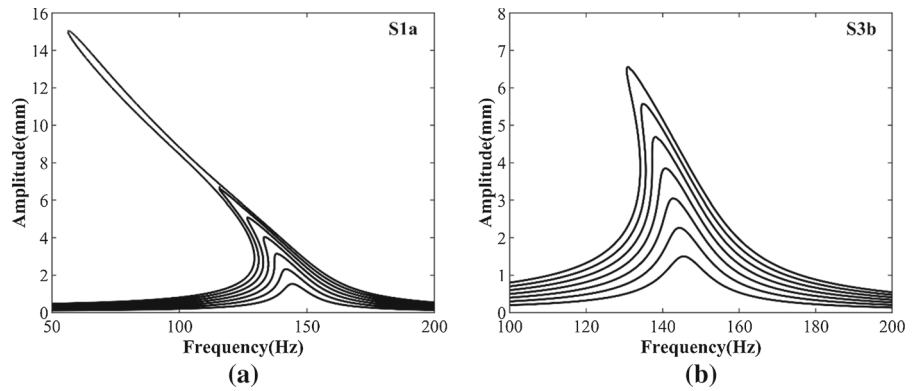
Fig. 7 Amplitudes at resonance frequency with various parameters of r_{12}: **a** S1a and **b** S3b

Fig. 8 Amplitudes at resonance frequency with various parameters of c_1 for S2b configuration

(LSWRM). With the adoption of MVP, the enforcement of the interface and boundary constraints is released. What's more, the discretized equations are convenient for numerical simulation. To obtain the time-domain response of the beam embedded with NiTi-ST, the domain decomposition is applied. The beam is decomposed into N subdomains on the x-direction, as shown in Fig. 9. Sub-coordinate $o' - \bar{x}$ is established in each subdomain.

The modified variational function Π is constructed as:
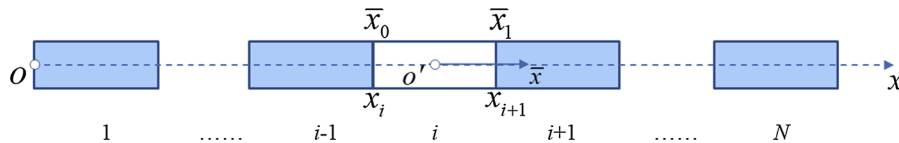
Fig. 9 Beam model discretized in the space domain

$$\Pi = \sum_{i=1}^{N} \left(T_i - U_i + W_{f,i} + W_{st,i} \right)$$
$$+ \sum_{i=1}^{N-1} \left(P_\lambda^{i,i+1} - P_\kappa^{i,i+1} \right) \tag{19}$$

where T_i, U_i, $W_{f,i}$, and $W_{st,i}$ are the kinetic energy, the strain energy, the work done by external loads, and the work done by the restoring and damping force provided by NiTi-ST, respectively. They can be easily obtained by replacing the general displacement w with the displacement of each segment w_i in Eq. (11). The subscript i represents the segment number. $P_\lambda^{i,i+1}$ and $P_\kappa^{i,i+1}$ are the potential energy of the virtual boundaries between the i and $i + 1$ segment, given as

$$P_\lambda^{i,i+1} = \left(\xi_w \sigma_w \Theta_w + \xi_r \sigma_r \Theta_r \right)\big|_{x=x_{i+1}} \tag{20}$$

$$P_\kappa^{i,i+1} = \frac{1}{2} \left(\xi_w \kappa_w \Theta_w^2 + \xi_r \kappa_r \Theta_r^2 \right)\big|_{x=x_{i+1}} \tag{21}$$

where Θ_w and Θ_r are the relevant continuity equations coordinating the displacements of two adjacent subdomains, written as:

$$\Theta_w = w_i - w_{i+1}, \quad \Theta_r = \frac{\partial w_i}{\partial x} - \frac{\partial w_{i+1}}{\partial x} \tag{22}$$

σ_w and σ_r are the Lagrange multipliers which can be recognized by setting the variation of Eq. (19) to zero:

$$\sigma_w = -\frac{\partial N_x}{\partial x}, \quad \sigma_r = N_x \tag{23}$$

ξ_w and ξ_r are the parameters controlling the boundary conditions. For two adjacent subdomains, the values of these parameters are set to be 1. For the real boundaries of the beam, the values are listed in Table 3.

To obtain the discretized governing equation of motion, the generalized displacement of each beam segment w_i is expanded with the Chebyshev

Table 3 Values of boundary controlling parameters for beam boundary conditions

Boundary condition	Constraints	ξ_w	ξ_r
Free	–	0	0
Simply supported	$w = 0$	1	0
Clamped	$w = \partial w/\partial x = 0$	1	1

orthogonal polynomial of the first kind (COPFK). The COPFK is given as

$$\psi_0(\bar{x}) = 1, \quad \psi_1(\bar{x}) = \bar{x},$$
$$\psi_i(\bar{x}) = 2\bar{x}\psi_i(\bar{x}) - \psi_{i-1}(\bar{x}) \tag{24}$$

where $\bar{x}$ is the local displacement of ith segment, given as $x = a_0\bar{x} + a_1$ with $a_0 = (x_{i+1} - x_i)/2$ and $a_1 = (x_{i+1} + x_i)/2$. Then, the displacement w_i can be written as

$$w_i(\bar{x}, t) = \sum_{j=0}^{P} \psi_i(\bar{x})w_{j,i}(t) = \boldsymbol{\psi}(x)\boldsymbol{w}_i(t) \tag{25}$$

with P being the maximum number of COPFK terms. Substituting Eqs. (20), (21) and (25) into Eq. (19) and performing the variational operation with respect to the generalized coordinate vector $\boldsymbol{w}$, one obtains the discretized governing equations of the composite beam embedded with NiTi-ST:

$$\mathbf{M}\ddot{\boldsymbol{q}} + \mathbf{C}\dot{\boldsymbol{q}} + (\mathbf{K} - \mathbf{K}_\lambda + \mathbf{K}_\kappa)\boldsymbol{q} = \mathbf{F}_w + \mathbf{F}_{st} \tag{26}$$

where $\boldsymbol{q}$ is the global generalized coordinate vector. $\mathbf{M}$ and $\mathbf{K}$ are, respectively, the disjoint generalized mass and stiffness matrices. $\mathbf{C}$ is the structural damping matrix of the composite beam, which is defined a s $\eta\mathbf{K}$, $\mathbf{K}_\lambda$ and $\mathbf{K}_\kappa$ are the generalized stiffness matrices introduced by the MVP and LSWRM, respectively. $\mathbf{F}_w$ and $\mathbf{F}_{st}$ are the generalized force vector of external loads and the nonlinear restoring and damping force provided by NiTi-ST. Setting the truncation order $N = 4$ and $P = 4$, the visualized patterns of $\mathbf{M}$, $\mathbf{K}$, $\mathbf{K}_\lambda$ and $\mathbf{K}_\kappa$ are presented in Fig. 10.

4.2 Numerical results in the time domain

Since Eq. (26) is a set of nonlinear ODEs, the Newmark-β method combined with direct iteration procedures is applied to obtain the time-domain responses. The parameters for Newmark-β method are: $\alpha = 0.25$, $\beta = 0.5$ and $\Delta t = 10^{-4}$ s. The initial generalized displacement velocity and acceleration vectors are set to be zero vectors.

The Newmark-β method with direct iteration procedure can be expressed as follows:

1. Ignore the nonlinear restoring and damping force vector. Start the Newmark-β procedure with the governing equation $\mathbf{M}\ddot{\boldsymbol{q}} + \mathbf{C}\dot{\boldsymbol{q}} + (\mathbf{K} - \mathbf{K}_\lambda + \mathbf{K}_\kappa)\boldsymbol{q} = \mathbf{F}_w$. Calculate the

Fig. 10 Visualized pattern of matrices in Eq. (26): **a M**, **b K**, **c $\mathbf{K}_\lambda$** and **d $\mathbf{K}_\kappa$**
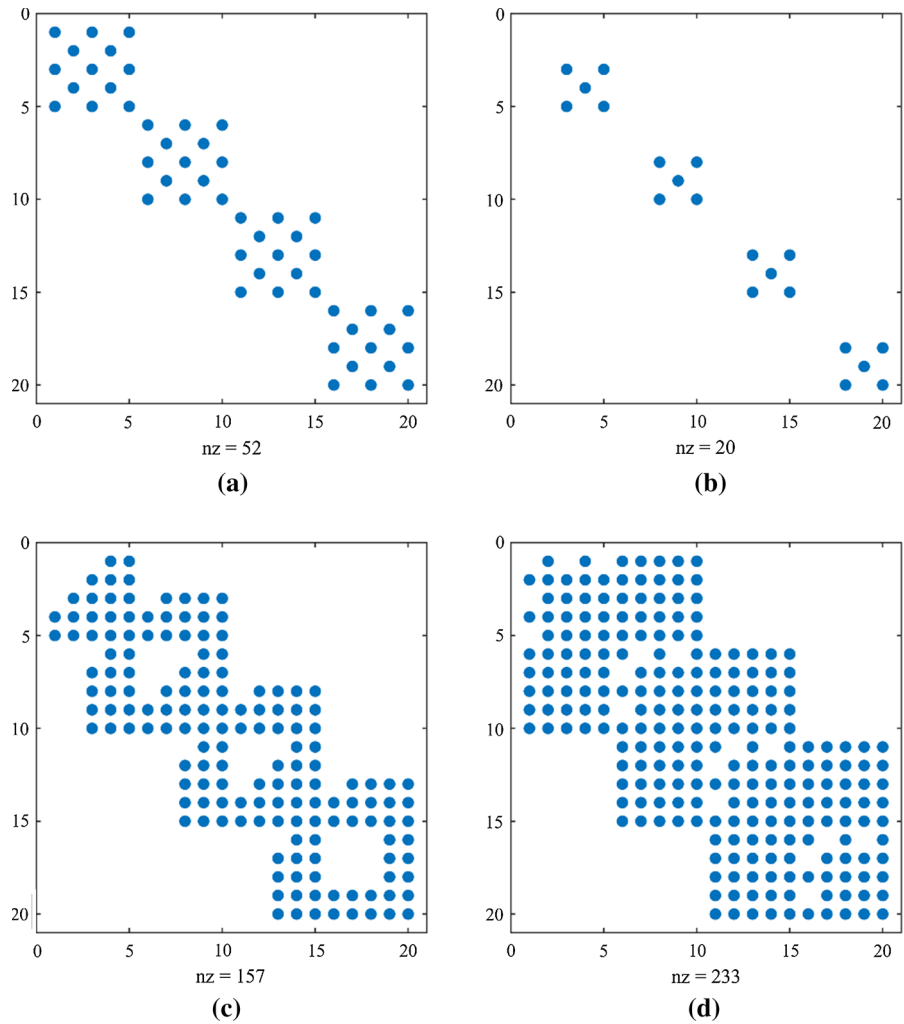

generalized coordinate vector $\boldsymbol{q}_{t+\Delta t}^i$ ($i \geq 1$) of the next Newmark step;

2. Start the direct iteration procedure. The nonlinear restoring and damping force $\mathbf{F}_{st}^i$ is related to $\boldsymbol{q}^i$. Calculate $\mathbf{F}_{st}^i$ with $\boldsymbol{q}^i$ from the previous step. Replace the governing equation with $\mathbf{M}\ddot{\boldsymbol{q}}^{i+1} + \mathbf{C}\dot{\boldsymbol{q}}^{i+1} + (\mathbf{K} - \mathbf{K}_\lambda + \mathbf{K}_\kappa)\boldsymbol{q}^{i+1} = \mathbf{F}_w + \mathbf{F}_{st}^i$, and start the Newmark-$\beta$ procedure again. The first nonlinear coordinate vector $\boldsymbol{q}^{i+1}$ can be obtained;

3. Repeat the iteration i times until $\left|\boldsymbol{q}^{i+1} - \boldsymbol{q}^i\right| < \varepsilon$. While the difference of the response in two adjacent iteration steps is smaller than the tolerance value, the response is considered to be the real nonlinear response of the step of the Newmark procedure.

4. Calculate the next Newmark step based on the previous nonlinear response until the whole procedure is over.

Figure 11 demonstrates the time history response of the composite beam embedded with different NiTi-ST and excited with 146.3 Hz harmonic load. The size of the excitation is 4 kPa, which is the same as the external load of Fig. 5a. The response is measured at the position of $3/4L$ on the x-axis. The results indicated that S1a and S3b configuration strongly reduced the amplitude of vibration to 11.93% and 12.20% near the resonance frequency. The S2b performs worst among all the NiTi-ST configurations with a suppression rate of 44.39%. Figure 12 shows the vibration suppression effect of the beam excited with 1000 Hz load. The

Fig. 11 Time-domain responses with excitations at 146.3 Hz of different configurations: **a** S1a, **b** S2a, **c** S2b, **d** S3a, **e** S3b and **f** S3c
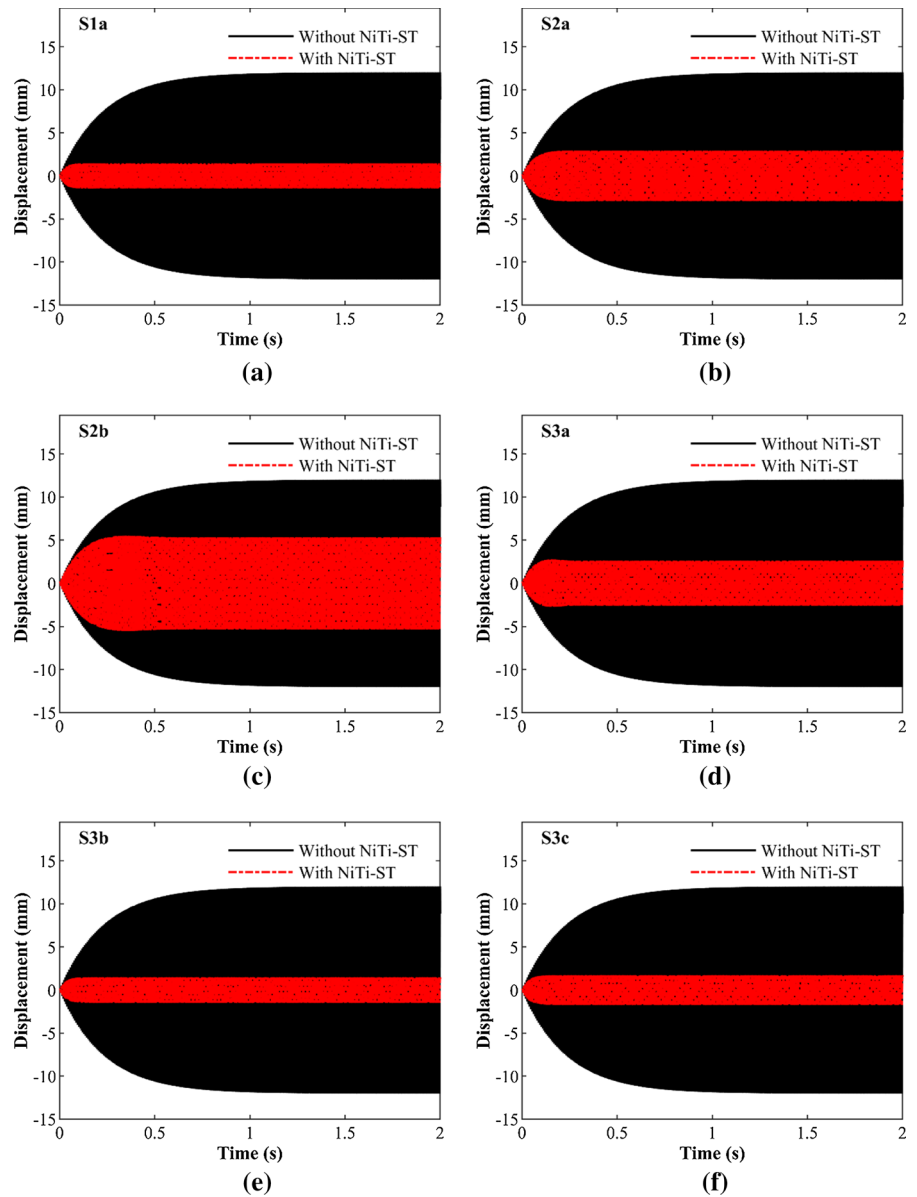
NiTi-ST can suppress the vibration rapidly at a higher frequency.

4.3 Verifications of semi-analytical and numerical results

The verifications are obtained via the Runge–Kutta method with a simulation time set to be long enough for a steady-state response. The amplitude is determined as the maximum absolute displacement in the last several periods of the time history. The numerical solutions are compared with the analytical results in Fig. 5b and yield good agreements, as shown in Fig. 13.

Good agreements of the numerical results can also be observed from Fig. 14. The domain decomposition method combined with the Newmark-beta method is proved to be a promising approach for nonlinear vibration analysis of continuum.

Fig. 12 Time-domain responses with excitations at 1000 Hz of different NiTi-ST configurations: **a** S1a, **b** S2a, **c** S2b, **d** S3a, **e** S3b and **f** S3c
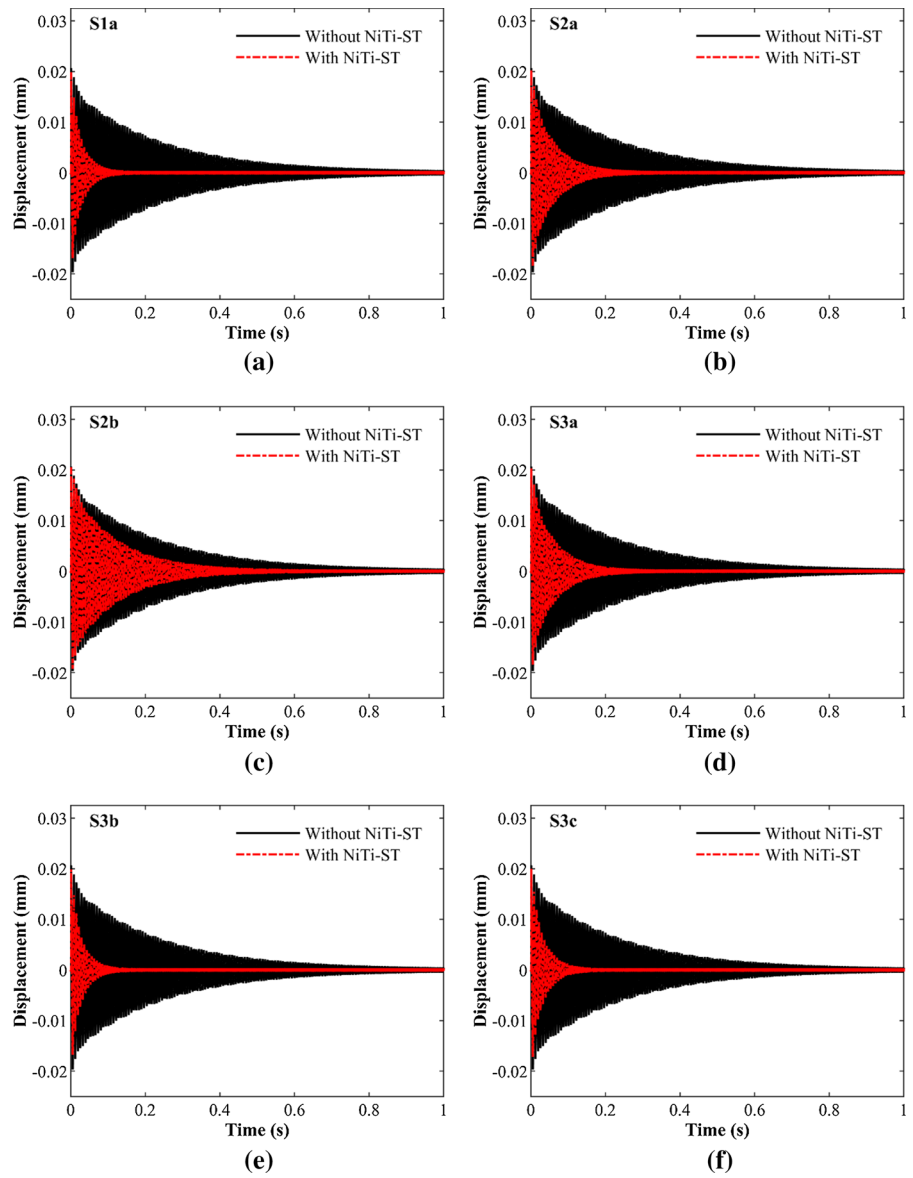

5 Conclusion

The present study was designed to determine the vibration suppression effect and nonlinear behavior of NiTi-ST coupled to a composite beam. According to the semi-analytical and numerical results, the NiTi-ST can greatly reduce the vibration of the composite beam under harmonic excitations. Differences between NiTi-ST configurations are revealed by the polynomial model. The minus cubic term of the model determines the softening behavior and can lead to instability. The polynomial models are suitable for reporting nonlinear responses under reasonable excitation. The linear damping term contributes to the
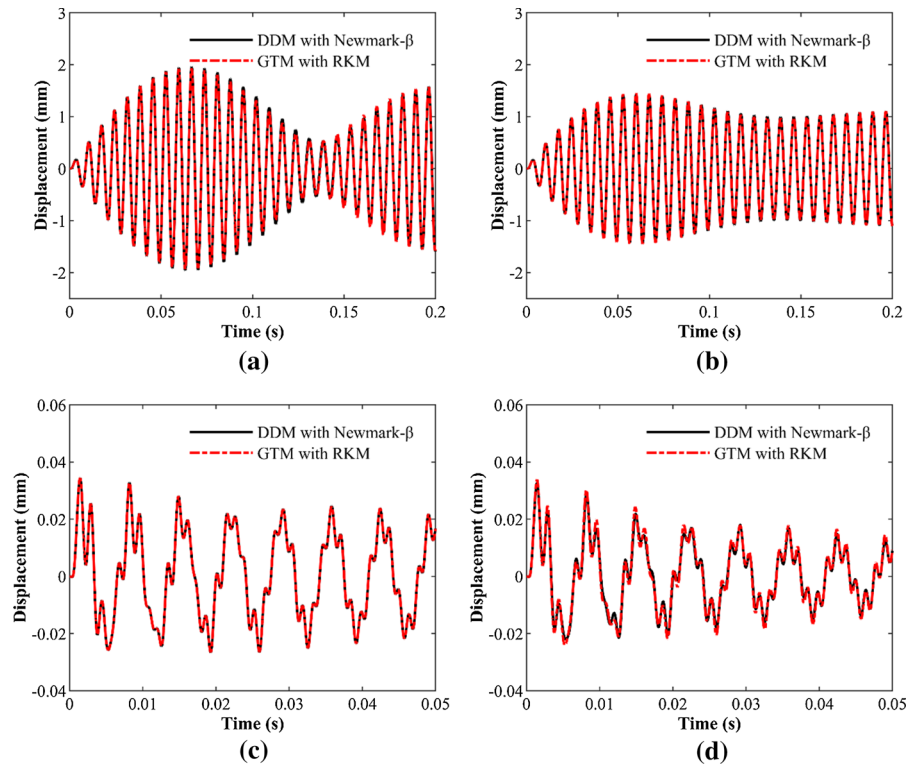
Fig. 13 Verifications of
semi-analytical results
presented in Fig. 5b
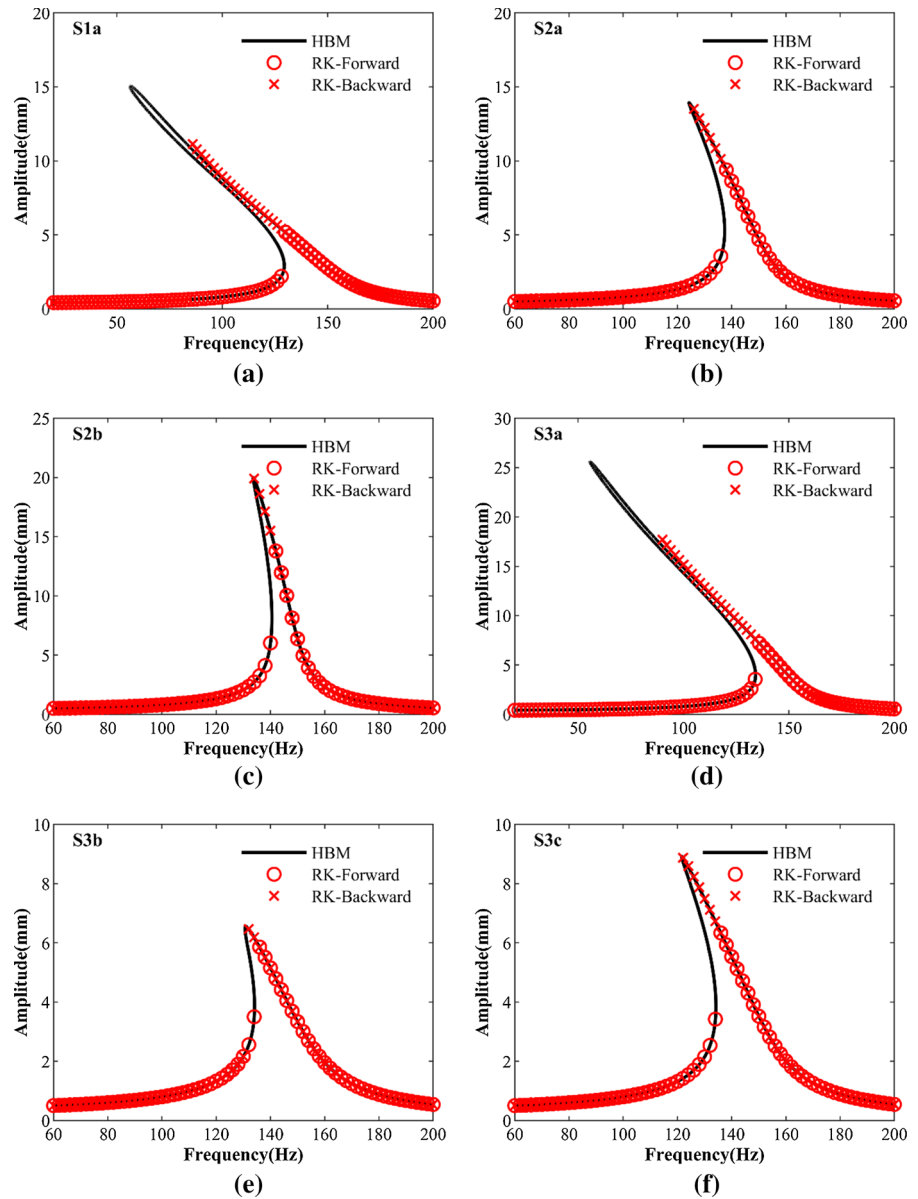
ability of vibration suppression. What's more, the ability of the domain decomposition method dealing with nonlinear vibration problems is proved. The numerical results achieved good agreements with the Runge–Kutta method. The domain decomposition method combined with the Newmark-β method shows great convenience in composite structures. Other structures such as plates, cylinder shells, and conical

shells embedded with NiTi-ST may also be analyzed with this method.

This work is just the beginning of vibration suppression using NiTi-ST. Unfortunately, the study carried out numerical verifications only. The thermo-mechanical coupling behavior of NiTi-ST is ignored. Further researches and experiments are required to determine the accuracy of this coupled model and

Fig. 14 Verification of time-domain numerical results with and without NiTi-ST: **a** at 143 Hz without NiTi-ST, **b** at 143 Hz with NiTi-ST, **c** at 760 Hz without NiTi-ST and **d** at 760 Hz with NiTi-ST

explore the practical vibration suppression application for more structures.

Authors' contributions All the authors conceived the project. L-HZ wrote the original draft. Y-WZ, HD, and L-QC reviewed the manuscript.

Availability of data and material Not applicable.

Code availability Not applicable.

Compliance with ethical standards

Conflicts of interest The authors declare that they have no conflict of interest.

References

1. Malatkar, P., Nayfeh, A.H.: Steady-state dynamics of a linear structure weakly coupled to an essentially nonlinear oscillator. Nonlinear Dyn. **47**(1), 167–179 (2007). https://doi.org/10.1007/s11071-006-9066-4

2. Oueini, S.S., Nayfeh, A.H., Pratt, J.R.: A nonlinear vibration absorber for flexible structures. Nonlinear Dyn. **15**(3), 259–282 (1998). https://doi.org/10.1023/A:1008250524547

3. Frank Pai, P., Schulz, M.J.: A refined nonlinear vibration absorber. Int. J. Mech. Sci. **42**(3), 537–560 (2000). https://doi.org/10.1016/S0020-7403(98)00135-0

4. Lo Feudo, S., Touzé, C., Boisson, J., Cumunel, G.: Nonlinear magnetic vibration absorber for passive control of a multi-storey structure. J. Sound Vib. **438**, 33–53 (2019). https://doi.org/10.1016/j.jsv.2018.09.007

5. Alujević, N., Čakmak, D., Wolf, H., Jokić, M.: Passive and active vibration isolation systems using inerter. J. Sound Vib. **418**, 163–183 (2018). https://doi.org/10.1016/j.jsv.2017.12.031

6. Afsharfard, A., Farshidianfar, A.: Design of nonlinear impact dampers based on acoustic and damping behavior. Int. J. Mech. Sci. **65**(1), 125–133 (2012). https://doi.org/10.1016/j.ijmecsci.2012.09.010

7. Geng, X., Ding, H., Wei, K., Chen, L.: Suppression of multiple modal resonances of a cantilever beam by an impact damper. Appl. Math. Mech. **41**(3), 383–400 (2020). https://doi.org/10.1007/s10483-020-2588-9

8. Sigalov, G., Gendelman, O.V., Al-Shudeifat, M.A., Manevitch, L.I., Vakakis, A.F., Bergman, L.A.: Resonance captures and targeted energy transfers in an inertially-coupled rotational nonlinear energy sink. Nonlinear Dyn. **69**(4),

1693–1704 (2012). https://doi.org/10.1007/s11071-012-0379-1

9. Motato, E., Haris, A., Theodossiades, S., Mohammadpour, M., Rahnejat, H., Kelly, P., Vakakis, A.F., McFarland, D.M., Bergman, L.A.: Targeted energy transfer and modal energy redistribution in automotive drivetrains. Nonlinear Dyn. **87**(1), 169–190 (2017). https://doi.org/10.1007/s11071-016-3034-4

10. Ding, H., Chen, L.-Q.: Designs, analysis, and applications of nonlinear energy sinks. Nonlinear Dyn. (2020). https://doi.org/10.1007/s11071-020-05724-1

11. Zhang, Y.-W., Hou, S., Zhang, Z., Zang, J., Ni, Z.-Y., Teng, Y.-Y., Chen, L.-Q.: Nonlinear vibration absorption of laminated composite beams in complex environment. Nonlinear Dyn. (2020). https://doi.org/10.1007/s11071-019-05442-3

12. Zhang, Y.-W., Lu, Y.-N., Zhang, W., Teng, Y.-Y., Yang, H.-X., Yang, T.-Z., Chen, L.-Q.: Nonlinear energy sink with inerter. Mech. Syst. Signal Process. **125**, 52–64 (2019). https://doi.org/10.1016/j.ymssp.2018.08.026

13. Xue, J., Zhang, Y., Ding, H., Chen, L.: Vibration reduction evaluation of a linear system with a nonlinear energy sink under a harmonic and random excitation. Appl. Math. Mech. **41**(1), 1–14 (2019). https://doi.org/10.1007/s10483-020-2560-6

14. Zhang, Y.-W., Zhang, Z., Chen, L.-Q., Yang, T.-Z., Fang, B., Zang, J.: Impulse-induced vibration suppression of an axially moving beam with parallel nonlinear energy sinks. Nonlinear Dyn. **82**(1), 61–71 (2015). https://doi.org/10.1007/s11071-015-2138-6

15. Chen, J.E., He, W., Zhang, W., Yao, M.H., Liu, J., Sun, M.: Vibration suppression and higher branch responses of beam with parallel nonlinear energy sinks. Nonlinear Dyn. **91**(2), 885–904 (2018). https://doi.org/10.1007/s11071-017-3917-z

16. Zhang, Y.-W., Zhang, H., Hou, S., Xu, K.-F., Chen, L.-Q.: Vibration suppression of composite laminated plate with nonlinear energy sink. Acta Astronaut. **123**, 109–115 (2016). https://doi.org/10.1016/j.actaastro.2016.02.021

17. Chen, J., Zhang, W., Yao, M., Liu, J., Sun, M.: Vibration reduction in truss core sandwich plate with internal nonlinear energy sink. Compos. Struct. **193**, 180–188 (2018). https://doi.org/10.1016/j.compstruct.2018.03.048

18. Chen, H.-Y., Mao, X.-Y., Ding, H., Chen, L.-Q.: Elimination of multimode resonances of composite plate by inertial nonlinear energy sinks. Mech. Syst. Signal Process. (2020). https://doi.org/10.1016/j.ymssp.2019.106383

19. Tian, W., Li, Y., Li, P., Yang, Z., Zhao, T.: Passive control of nonlinear aeroelasticity in hypersonic 3-D wing with a nonlinear energy sink. J. Sound Vib. **462**, 114942 (2019). https://doi.org/10.1016/j.jsv.2019.114942

20. Ozbulut, O.E., Hurlebaus, S., Desroches, R.: Seismic response control using shape memory alloys: a review. J. Intell. Mater. Syst. Struct. **22**(14), 1531–1549 (2011). https://doi.org/10.1177/1045389X11411220

21. Paiva, A., Savi, M.A.: An overview of constitutive models for shape memory alloys. Math. Probl. Eng. (2006). https://doi.org/10.1155/MPE/2006/56876

22. Machado, L.G., Savi, M.A., Pacheco, P.M.C.L.: Nonlinear dynamics and chaos in coupled shape memory oscillators.

Int. J. Solids Struct. **40**(19), 5139–5156 (2003). https://doi.org/10.1016/S0020-7683(03)00260-9

23. Savi, M.A.: Nonlinear dynamics and chaos in shape memory alloy systems. Int. J. Non-linear Mech. **70**, 2–19 (2015). https://doi.org/10.1016/j.ijnonlinmec.2014.06.001

24. Ghasemi, M.R., Shabakhty, N., Enferadi, M.H.: Vibration control of offshore jacket platforms through shape memory alloy pounding tuned mass damper (SMA-PTMD). Ocean Eng. **191**, 106348 (2019). https://doi.org/10.1016/j.oceaneng.2019.106348

25. Kumbhar, S.B., Chavan, S.P., Gawade, S.S.: Adaptive tuned vibration absorber based on magnetorheological elastomer-shape memory alloy composite. Mech. Syst. Signal Process. **100**, 208–223 (2018). https://doi.org/10.1016/j.ymssp.2017.07.027

26. Huang, H., Chang, W.-S.: Application of pre-stressed SMA-based tuned mass damper to a timber floor system. Eng. Struct. **167**, 143–150 (2018). https://doi.org/10.1016/j.engstruct.2018.04.011

27. Qian, H., Li, H., Song, G.: Experimental investigations of building structure with a superelastic shape memory alloy friction damper subject to seismic loads. Smart Mater. Struct. **25**(12), 125026 (2016). https://doi.org/10.1088/0964-1726/25/12/125026

28. Lester, B.T., Baxevanis, T., Chemisky, Y., Lagoudas, D.C.: Review and perspectives: shape memory alloy composite systems. Acta Mech. **226**, 3907–3960 (2015). https://doi.org/10.1007/s00707-015-1433-0

29. Alebrahim, R., Sharifishourabi, G., Sharifi, S., Alebrahim, M., Zhang, H., Yahya, Y., Ayob, A.: Thermo-mechanical behaviour of smart composite beam under quasi-static loading. Compos. Struct. **201**, 21–28 (2018). https://doi.org/10.1016/j.compstruct.2018.06.023

30. Bayat, Y., EkhteraeiToussi, H.: A nonlinear study on structural damping of SMA hybrid composite beam. Thin-Walled Struct. **134**, 18–28 (2019). https://doi.org/10.1016/j.tws.2018.09.041

31. Bayat, Y., EkhteraeiToussi, H.: Damping capacity in pseudo-elastic and ferro-elastic shape memory alloy-reinforced hybrid composite beam. J. Reinf. Plast. Compos. **38**(10), 467–477 (2019). https://doi.org/10.1177/0731684418825001

32. Soltanieh, G., Kabir, M.Z., Shariyat, M.: A robust algorithm for behavior and effectiveness investigations of super-elastic SMA wires embedded in composite plates under impulse loading. Compos. Struct. **179**, 355–367 (2017). https://doi.org/10.1016/j.compstruct.2017.07.065

33. Tinker, M.L., Cutchins, M.A.: Damping phenomena in a wire rope vibration isolation system. J. Sound Vib. **157**(1), 7–18 (1992). https://doi.org/10.1016/0022-460X(92)90564-E

34. Gerges, R.R., Vickery, B.J.: Parametric experimental study of wire rope spring tuned mass dampers. J. Wind Eng. Ind. Aerodyn. **91**(12), 1363–1385 (2003). https://doi.org/10.1016/j.jweia.2003.09.038

35. Carboni, B., Lacarbonara, W.: A new vibration absorber based on the hysteresis of multi-configuration NiTiNOL-steel wire ropes assemblies. In: MATEC Web of Conferences vol 16 (2014). https://doi.org/https://doi.org/10.1051/matecconf/20141601004

36. Carboni, B., Lacarbonara, W., Auricchio, F.: Hysteresis of multiconfiguration assemblies of NiTiNOL and steel strands: experiments and phenomenological identification. J. Eng. Mech. (2015). https://doi.org/10.1061/(asce)em.1943-7889.0000852

37. Mohsenian, A., Zakerzadeh, M., Shariat Panahi, M., Fakhrzade, A.: Modeling SMA actuated systems based on Bouc–Wen hysteresis model and feed-forward neural network. J. Comput. Appl. Mech. 49(1), 9–17 (2018). https://doi.org/10.22059/JCAMECH.2017.234999.151

38. Hassani, V., Tjahjowidodo, T., Do, T.N.: A survey on hysteresis modeling, identification and control. Mech. Syst. Signal Process. 49(1–2), 209–233 (2014). https://doi.org/10.1016/j.ymssp.2014.04.012

39. Ismail, M., Ikhouane, F., Rodellar, J.: The hysteresis Bouc–Wen model, a survey. Arch. Comput. Methods Eng. 16(2), 161–188 (2009). https://doi.org/10.1007/s11831-009-9031-8

40. Carboni, B., Lacarbonara, W.: Nonlinear dynamic characterization of a new hysteretic device: experiments and computations. Nonlinear Dyn. 83(1–2), 23–39 (2015). https://doi.org/10.1007/s11071-015-2305-9

41. Carboni, B., Lacarbonara, W.: Nonlinear vibration absorber with pinched hysteresis: theory and experiments. J. Eng. Mech. (2016). https://doi.org/10.1061/(asce)em.1943-7889.0001072

42. Zhang, Y., Xu, K., Zang, J., Ni, Z., Zhu, Y., Chen, L.: Dynamic design of a nonlinear energy sink with NiTiNOL-steel wire ropes based on nonlinear output frequency response functions. Appl. Math. Mech. 40(12), 1791–1804 (2019). https://doi.org/10.1007/s10483-019-2548-9

43. Carboni, B., Lacarbonara, W., Brewick, P.T., Masri, S.F.: Dynamical response identification of a class of nonlinear hysteretic systems. J. Intell. Mater. Syst. Struct. 29(13), 2795–2810 (2018). https://doi.org/10.1177/1045389x18778792

44. Brewick, P.T., Masri, S.F., Carboni, B., Lacarbonara, W.: Data-based nonlinear identification and constitutive modeling of hysteresis in NiTiNOL and steel strands. J. Eng. Mech. (2016). https://doi.org/10.1061/(asce)em.1943-7889.0001170

45. Brewick, P.T., Masri, S.F., Carboni, B., Lacarbonara, W.: Enabling reduced-order data-driven nonlinear identification and modeling through naïve elastic net regularization. Int. J. Non-linear Mech. 94, 46–58 (2017). https://doi.org/10.1016/j.ijnonlinmec.2017.01.016

46. Lacarbonara, W., Bernardini, D., Vestroni, F.: Nonlinear thermomechanical oscillations of shape-memory devices. Int. J. Solids Struct. 41(5–6), 1209–1234 (2004). https://doi.org/10.1016/j.ijsolstr.2003.10.015

47. Bernardini, D., Rega, G.: Evaluation of different SMA models performances in the nonlinear dynamics of pseudoelastic oscillators via a comprehensive modeling framework. Int. J. Mech. Sci. 130, 458–475 (2017). https://doi.org/10.1016/j.ijmecsci.2017.06.023

48. Luo, A.C.J., Huang, J.: Approximate solutions of periodic motions in nonlinear systems via a generalized harmonic balance. J. Vib. Control 18(11), 1661–1674 (2011). https://doi.org/10.1177/1077546311421053

49. Ye, S.-Q., Mao, X.-Y., Ding, H., Ji, J.-C., Chen, L.-Q.: Nonlinear vibrations of a slightly curved beam with nonlinear boundary conditions. Int. J. Mech. Sci. (2020). https://doi.org/10.1016/j.ijmecsci.2019.105294

50. Qu, Y., Chen, Y., Long, X., Hua, H., Meng, G.: A variational method for free vibration analysis of joined cylindrical-conical shells. J. Vib. Control 19(16), 2319–2334 (2012). https://doi.org/10.1177/1077546312456227

51. Qu, Y., Chen, Y., Long, X., Hua, H., Meng, G.: A modified variational approach for vibration analysis of ring-stiffened conical–cylindrical shell combinations. Eur. J. Mech. A/Solids 37, 200–215 (2013). https://doi.org/10.1016/j.euromechsol.2012.06.006